Electric field induced large Rashba effect and topological phase transition in halide perovskite superlattices

Xinyu Wang,[1,2] Xu Li,[1,2] Hao Tian,[3] Hai Sang,[1] Jian Zhou,[1,2] Lan Chen,[1,2,4] Hong Jian Zhao,[5] Di Wu,[1,2] Haijun Zhang,[1] Laurent Bellaiche,[6] Jun-Ming Liu,[1] and Yurong Yang[1,2,*]

[1]*Laboratory of Solid State Microstructures, Nanjing University, Nanjing 210093, China*

[2]*Jiangsu Key Laboratory of Artificial Functional Materials, Department of Materials Science and Engineering, Nanjing University, Nanjing 210093, China*

[3]*School of Physics and Electronic Engineering, Zhengzhou Normal University, Zhengzhou 450044, China*

[4]*Nantong Institute of Material Engineering Technology, Nanjing University, Nantong 226001, China*

[5]*International Center for Computational Method and Software, College of Physics, Jilin University, Changchun 130012, China*

[6]*Physics Department, Institute for Nanoscience and Engineering, University of Arkansas, Fayetteville, Arkansas 72701, USA*

(Received 1 December 2022; revised 9 April 2023; accepted 5 June 2023; published 11 July 2023)

We introduce superlattices made of ferroelectric halide perovskites as a class of functional materials possessing large Rashba effect and phase transition from normal insulator (NI) to topological insulator (TI) induced by an electric field. Using first-principles methods, in $CsPbI_3/CsSiI_3$ and $CsSnI_3/CsSiI_3$ superlattices, we found a nonmonotonic Rashba parameter with respect to the magnitude of polarization and large maximal Rashba effect at a critical polarization, where the phase transition from NI to TI occurs when changing the polarization. This phase transition and the large maximal Rashba effect are related to band-gap engineering under an electric field. In contrast to traditional nonpolar TIs, in these ferroelectric TIs, the energy level of the Dirac point and the spin texture of surface states are largely tunable by changing polarization or strain. Our results thus highlight the interplay among ferroelectricity, Rashba effect, and topological order in a single material, which is promising toward electronic and spintronic applications.

DOI: 10.1103/PhysRevB.108.045114

I. INTRODUCTION

Topological insulator (TI) states [1–5] and Rashba-type effects [6–10] are among the most interesting current phenomena in condensed matter physics, as a result of relativistic interaction of spin-orbit coupling (SOC). TIs, exhibiting robust edge/surface currents and spin-momentum locking, provide platforms for various fundamental exciting research, including magnetic monopoles [11], Majorana fermions [12], and the application of fault-tolerant quantum computing [13,14]. Bulk Rashba-type spin splitting, which occurs in materials/interface with breaking spatial inversion symmetry, can lead to spin Hall effect [15–17], spin interference [18,19], and spin-to-charge current interconversions [20,21]. Both topological phase and Rashba effects present strong spin-momentum locking, in principle providing the possibility of electric field control of electronic spins by manipulating topological order and Rashba effects. Ferroelectric materials are ideal candidates for controlling the topological order and Rashba effects via an electric field. Recently, the linear Rashba effect with polarization has been extensively studied in ferroelectrics [22–25]. Promisingly, topological order can also exist in ferroelectrics, for example, the hexagonal ABC hyperferroelectrics, antiferroelectrics [26,27], and the heterostructures consisting of TIs and ferroelectrics [28–30]. These discoveries highlight the possibility of simultaneously controlling the Rashba effect and the topological state by an electric field in a nonvolatile way in ferroelectrics. On the other hand, the ferroelectric materials possessing topological order discovered recently are nonperovskite structures. In the prototypical ferroelectric perovskite structure for which the designing and producing technology have been well developed, the topological orders have never been measured, and therefore, simultaneously tuning the topological order and the Rashba effect by an electric field has not been realized. One therefore still needs to find possible materials simultaneously hosting Rashba effects and topological order that are tunable by an electric field.

Iodide perovskites (ABI_3) are candidates for that since they hold large SOC due to the heavy element of iodine and ferroelectric properties as a result of perovskites having the possibility to be ferroelectrics [31–38]. Both $CsPbI_3$ and $CsSnI_3$ adopt the *Pnma* perovskite phase for their ground state with in-plane antipolar distortion [39,40]. On the other hand, the ground state of $CsSiI_3$ adopts a perovskite structure with *R*3*m* symmetry [22,41–43]. One can easily imagine that the perovskite $CsPbI_3/CsSiI_3$ and $CsSnI_3/CsSiI_3$ superlattices will possess structural distortion with either *Pnma* or/and *R*3*m* type distortion. We thus investigated the short-period [1/1] iodide perovskite superlattices made of $CsPbI_3/CsSiI_3$ and $CsSnI_3/CsSiI_3$ by first principles. These superlattices are indeed found to possess a large Rashba effect, which even shows anomalous behavior with the change of polar distortion. A transition from normal insulator (NI) to TI by an electric field is also presently predicted, along with a large Rashba effect

*yangyr@nju.edu.cn

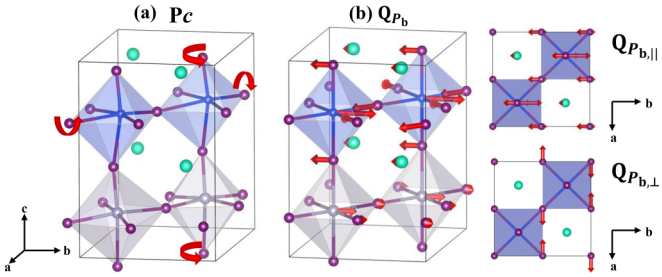

FIG. 1. (a) Atomic structure of $CsSnI_3/CsSiI_3$ superlattice with a space group *Pc*. (b) In-plane polar mode Q_{P_b} made by the ionic motions parallel to the **b** direction ($Q_{P_{b,||}}$) and perpendicular to the **b** direction ($Q_{P_{b,\perp}}$). The arrows in (a) represent the iodine octahedron rotation and tilting. Green, blue, gray, and purple balls represent Cs, Si, Sn, and I atoms, respectively.

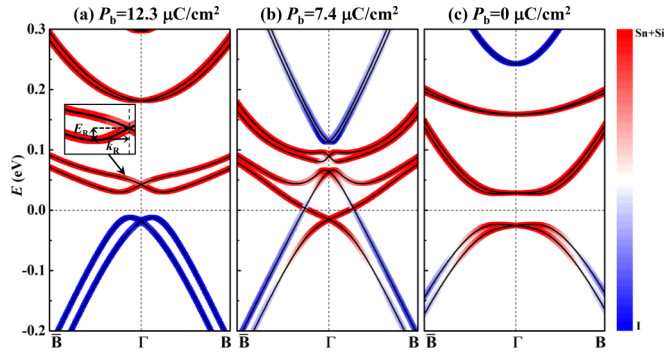

FIG. 2. The band structures of $CsSnI_3/CsSiI_3$ superlattice with in-plane polarization of (a) $P_b = 12.3\ \mu C/cm^2$, (b) $P_b = 7.4\ \mu C/cm^2$, and (c) $P_b = 0\ \mu C/cm^2$. The red and blue colors represent the corresponding states mainly coming from Si/Sn and I ions, respectively. In the inset of (a), we report the graphical definition of the Rashba momentum offset k_R and the Rashba energy splitting E_R.

at the critical field for which the NI-to-TI transition occurs. Moreover, the Dirac point in the bulk band gap can be shifted by an electric field and strain, even crossing the Fermi level. Consequently, the spin texture of the surface state is tunable by an electric field. Our results therefore provide a powerful and convenient way to tune topological order and the Rashba effect.

II. METHODS

Density functional theory (DFT) calculations are performed using VASP with the projector augmented-wave method [44,45]. An energy cutoff of 320 eV, a *k*-point grid size of $8 \times 8 \times 6$, and the Perdew-Burke-Ernzerhof parametrization revised for solids (PBEsol) functional [46] are used in all the calculations. We further performed calculations using the HSE hybrid functional [47] to confirm the robustness of the PBEsol functional in the Supplemental Material [48]. Atomic structural relaxations were carried out until the force on each atom was < 0.001 eV Å^{-1}, and the energy convergence criterion of 10^{-8} eV was adopted. The calculations are performed in the iodide perovskite superlattices of $[CsPbI_3]_1/[CsSiI_3]_1$ and $[CsSnI_3]_1/[CsSiI_3]_1$, where one unit layer of $CsSiI_3$ and one unit layer of $CsPbI_3$ or $CsSnI_3$ successively alternate along the pseudocubic [001] direction (see Fig. 1). A supercell with 20 atoms is used in DFT calculations, in which the lattice vectors are $\mathbf{a} = a(\mathbf{x} + \mathbf{y})$, $\mathbf{b} = b(-\mathbf{x} + \mathbf{y})$, and $\mathbf{c} = c\mathbf{z}$, where *a*, *b*, and *c* are related to the magnitude of the lattice constants and **x**, **y**, are **z** are unit vectors along the pseudocubic [100], [010], and [001] directions, respectively. Ferroelectric polarizations are calculated by using Born effective charge and atomic displacements. Tight-binding analysis with the WANNIER90 package was further performed for the calculation of topological phases [49,50]. The *s*- and *p*-orbital basis was used to construct the tight-binding Hamiltonian, and the topological indices were calculated by tracking hybrid Wannier charge centers using the WANNIERTOOLS package [51].

III. RESULTS AND DISCUSSION

The calculations confirm that $CsPbI_3/CsSiI_3$ with space group of $P2_1$ and $CsSnI_3/CsSiI_3$ with space group of *Pc* both possess an octahedral tilting type of $a^- a^- c^+$ pattern (using Glazer notation [52]) with out-of-phase in-plane octahedral tilting and in-phase of out-of-plane octahedral tilting (see Figs. S1(a) and S1(b) in the Supplemental Material [48]), and in-plane polar distortion (Q_{P_b}) with B-site cations moving along the **b** direction, while I anions move along the **a** and **b** directions [see Fig. 1(b)]. The in-plane polarizations for $CsPbI_3/CsSiI_3$ and $CsSnI_3/CsSiI_3$ are found to be 16.1 and 12.3 μC/cm^2, respectively. The major structural difference between $CsPbI_3/CsSiI_3$ and $CsSnI_3/CsSiI_3$ is that the latter additionally possesses another polar distortion along the **c** direction (Q_{P_c}, see Fig. S1(c) in the Supplemental Material [48]), with a polarization of 8.2 μC/cm^2, like the structure of $BiInO_3$ [53]. The structural similarity of iodine octahedral tilting and in-plane polarization in the two superlattices may lead to some electrical properties being similar.

Because of the polar symmetry and the large SOC associated with the heavy elements of I and Sn, the electronic structure of this superlattice shows that Rashba-type splittings occur along the Γ-*B* line in the Brillouin zone [see Fig. 2(a)]. The Rashba energy for the highest valence bands (HVBs) is 6.3 meV, and it is 12.7 meV for the lowest conduction bands (LCBs). The Rashba parameters ($\alpha_R = 2E_R/k_0$) of the HVB and LCB are 1.38 and 1.44 eV Å, respectively. The band gap for $CsSnI_3/CsSiI_3$ is rather small (i.e., 48 meV). Such a small gap can likely be engineered to vanish [54] by changing the polarization. Therefore, it is legitimate to wonder whether such a gap closing (if it occurs) can be accompanied by a topological transition.

Figures 2(b) and 2(c) show the band structures of $CsSnI_3/CsSiI_3$ with the reduced in-plane polarizations (P_b) of 7.4 and 0 μC/cm^2, respectively (the structures with reduced polarization are constructed by reducing the magnitude of the polar mode Q_{P_b}). As shown in Fig. 2, one can see that the band gap indeed decreases from 48 to 0 meV when the polarization decreases from 12.3 to 7.4 μC/cm^2 and then reopens when the polarization is < 7.4 μC/cm^2. The band gap increases to 50 meV when P_b further decreases to zero. In the band structure of $CsSnI_3/CsSiI_3$ with $P_b > 7.4\ \mu C/cm^2$ [see Fig. 2(a)], the HVBs near the Γ point are dominated by I−5*p* states, while the conduction bands near the Fermi level are mainly from

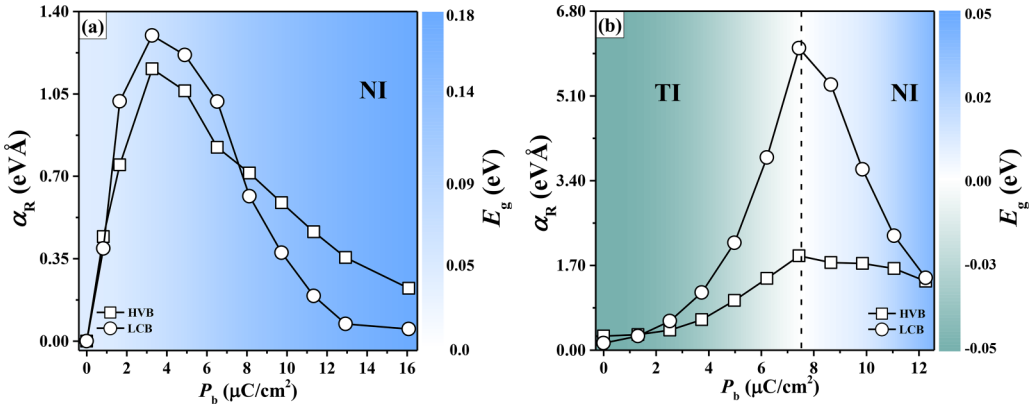

FIG. 3. Band gap and Rashba parameters of (a) $CsPbI_3/CsSiI_3$ and (b) $CsSnI_3/CsSiI_3$ as a function of the in-plane polarization P_b. The blue and green color contours represent the band gap.

the B site (Sn−5p and Si−3p). In contrast, the HVBs at the Γ point come from the B site (Sn−5p and Si−3p), while the third LCBs at the Γ point are dominated by I−5p states when the polarization is $< 7.4\,\mu C/cm^2$ [see Fig. 2(c)]. These band structures clearly show a band inversion induced by decreasing the in-plane polarization. Thus, the NI-TI transition of $CsSnI_3/CsSiI_3$ occurs when the polarization is $< 7.4\,\mu C/cm^2$. To further confirm this TI state, we calculated the topological invariant $\mathbb{Z}_2$ which is (1;000), thus indicating that it is indeed a strong TI.

We then consider the Rashba effect of the studied superlattices when changing the polarization. Figure 3 displays the Rashba parameters and band gaps as a function of polarization P_b in $CsPbI_3/CsSiI_3$ and $CsSnI_3/CsSiI_3$ superlattices. The band gap of $CsPbI_3/CsSiI_3$ monotonically decreases from 180 to 60 meV when decreasing the polarization from 16.1 to 0 $\mu C/cm^2$. It is consistent with the fact that the polar distortion (polarization) of the perovskite structure widens its band gap by allowing band edge orbitals to mix and repel each other [55,56]. Rashba parameters first increase from 0.2 to 1.2 eV Å for HVB and from 0.05 to 1.3 eV Å for LCB, respectively, when decreasing the polarization from 16.1 to 3.3 $\mu C/cm^2$. As the polarization further decreases to zero, Rashba parameters of both HVB and LCB sharply decrease to zero. This nonmonotonic phenomenon of Rashba parameters with respect to polarization is different from those reported in the literature where the Rashba parameter is linear with polarization (as found for GeTe, BrF_5, $BiAlO_3$, and $SrTiO_3$ [23–25,57]). We construct an effective two-band Hamiltonian with respect to the $P2_1$ space group (around the Γ point of the Brillion zone), incorporating various degrees of freedom, namely, the electronic polarization P_b (i.e., along the y direction), electronic momentum k_α (α=x, y, z), and electronic spin characterized by the Pauli matrices σ_β (β=x, y, z). The Hamiltonian is written as $H_R = E_0 + \lambda_{xx}k_x\sigma_x + \lambda_{xz}k_x\sigma_z + \lambda_{yy}k_y\sigma_y + \lambda_{zx}k_z\sigma_x + \lambda_{zz}k_z\sigma_z$. The corresponding eigenvalue and spin-splitting magnitude are given by $E_R = E_0 \pm \sqrt{(\lambda_{xx}k_x + \lambda_{zx}k_z)^2 + (\lambda_{yy}k_y)^2 + (\lambda_{xz}k_x + \lambda_{zz}k_z)^2}$, where $\lambda_{a\beta}$ (α, β=x, y, z) are parameters characterizing spin-splitting terms, $\lambda_{\alpha\beta} = \lambda_{\alpha\beta1}P_b + \lambda_{\alpha\beta3}P_b^3 + \lambda_{\alpha\beta5}P_b^5 + \cdots$). Figures S3(a)–S3(c) in the Supplemental Material [48] show the band structures around the Γ point along k_x, k_z, and k_y, respectively. Our model coincides with the band structures from DFT calculations. The phenomena of Rashba parameters evolve in a nonlinear manner with respect to the polarization P_b, indicating that the $\lambda_{\alpha\beta3}$ and $\lambda_{\alpha\beta5}$ coefficients are not negligible in halide superlattice, unlike the situation of various conventional Rashba materials. As a matter of fact, the nonmonotonic behavior can also be understood from the special in-plane polar mode in the superlattice. As shown in Fig. 1(b), the in-plane polar mode Q_{P_b} can be decomposed into two components, $Q_{P_{b,\parallel}}$ and $Q_{P_{b,\perp}}$ that are associated with atomic motions being parallel and perpendicular to the **b** direction, respectively. Both $Q_{P_{b,\parallel}}$ and $Q_{P_{b,\perp}}$ contribute to the in-plane polarization along the **b** direction as well as to the Rashba effect. Here, $Q_{P_{b,\parallel}}$ gives rise to a negative Rashba parameter, while $Q_{P_{b,\perp}}$ results in a positive one (see Fig. S4 in the Supplemental Material [48]). These two opposite contributions yield nonmonotonic behavior of the total Rashba parameter with respect to the polarization.

Figure 3(b) shows the band gap and Rashba parameters of $CsSnI_3/CsSiI_3$ as a function of polarization P_b. The band gap first decreases to zero when P_b decreases from 12.3 to 7.4 $\mu C/cm^2$ and then reopens from 0 to ∼ 50 meV when further decreasing P_b from 7.4 to 0 $\mu C/cm^2$. At $P_b = 7.4\,\mu C/cm^2$, the NI-TI phase transition occurs (also see Fig. 2) and TI states for $P_b < 7.4\,\mu C/cm^2$ are strong TIs with topological invariant $\mathbb{Z}_2$ of (1;000). The Rashba parameters of $CsSnI_3/CsSiI_3$ show nonmonotonic behavior as a function of the polarization. The maximum of the Rashba parameters is ∼ 6 eVÅ at the critical polarization, thus enhanced three times as compared with the Rashba parameter of the superlattice without reducing polarization and comparable with the largest Rashba parameter of 6.8 eV Å in SnTe reported in literature [58]. This increase of the Rashba parameter not only comes from the competition between the contributions of the two components of the polar modes (Fig. S4 in the Supplemental Material [48]) but also the fact that the HVB and LCB are symmetrically of the same character and therefore very effectively couple with each other through a Rashba-type Hamiltonian [59,60] $\Delta\varepsilon_m(\mathbf{k}) = \frac{\hbar}{m_0}\sum_{n\neq m}\frac{\langle u_m|H|u_n\rangle\langle u_n|\mathbf{q}\cdot\mathbf{p}|u_m\rangle + \text{c.c.}}{\varepsilon_m - \varepsilon_n}$, where u_i and ε_i are the eigenstate and eigenenergy corresponding to the state i at $\mathbf{k}_0$, respectively, $\mathbf{q} = \mathbf{k} - \mathbf{k}_0$, $\mathbf{p}$ denotes the

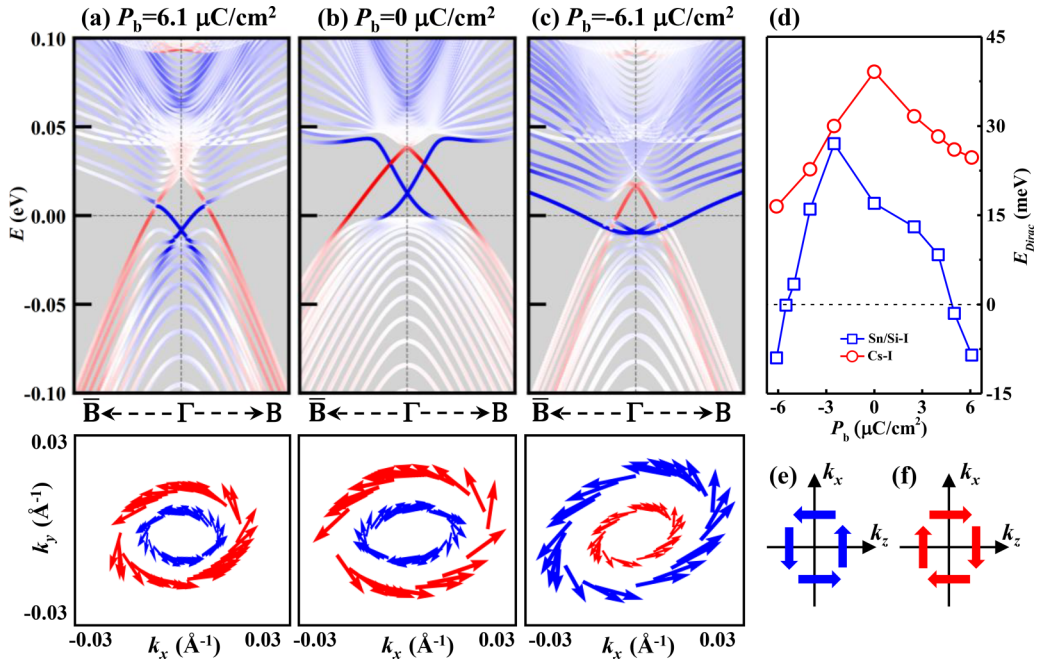

FIG. 4. Polarization effect on surface states. Band structure of $CsSnI_3/CsSiI_3$ superlattice in a (100) slab geometry with the in-plane polarization of (a) $P_b = 6.1\,\mu C/cm^2$, (b) $P_b = 0\,\mu C/cm^2$, and (c) $P_b = -6.1\,\mu C/cm^2$. The bottom panels of (a)–(c) display the corresponding spin texture of surface states near the Fermi level. (d) The energies of the two Dirac points as a function of P_b. The sketches of the spin texture for Rashba effect with (e) $P_b = 6.1\,\mu C/cm^2$ and (f) $P_b = -6.1\,\mu C/cm^2$, respectively.

momentum operator, H is the corresponding Hamiltonian for Rashba-type-splitting, and c.c. stands for complex conjugate. Therefore, the spin splitting clearly depends on the energy difference between the state m and its neighboring state n. In the band structure of $CsSnI_3/CsSiI_3$, the state m can be HVB or LCB. The energy difference $(\varepsilon_m - \varepsilon_n)$ between the m state (HVB or LCB) and its neighboring states decreases, and $\Delta\varepsilon_m$ thus increases. At the critical polarization for which the band gap is closed, $\varepsilon_m - \varepsilon_n$ is almost zero, and their Rashba splitting reaches its maximum.

We now consider the surface state of the TI phase in the $CsSnI_3/CsSiI_3$ superlattice. The energy variation of the $CsSnI_3/CsSiI_3$ superlattice along the path connecting the noncentrosymmetric to the centrosymmetric direction shows a low ferroelectric switching barrier (in Fig. S2 in the Supplemental Material [48]), indicating that the ferroelectric polarization can be switched by an electric field. Figures 4(a)–4(c) show the band structures and corresponding spin textures of surface states for $P_b = 6.1$, 0, and $-6.1\,\mu C/cm^2$, respectively. There are two nonequivalent Dirac cones which come from the Sn/Si-I termination and Cs-I termination (100) surfaces of the geometry slab, which contrast with the degenerate Dirac points in nonpolar TI structures [2,3,61]. For the case of $P_b = 6.1\,\mu C/cm^2$ shown in Fig. 4(a), the Dirac point from the Cs-I termination (red color) is above the Fermi level and buried in the continuum of bulk conduction states. The Dirac point from the Sn/Si-I termination (blue color) is below the Fermi level. Spin textures of the two surface states show the same chirality [bottom panel of Fig. 4(a)]. For the superlattice with zero polarization, the surface bands and Dirac points shift to higher energy than the case of $P_b = 6.1\,\mu C/cm^2$ [Fig. 4(b)]. Both Dirac points from Cs-I and Sn/Si-I terminations are above the Fermi level, leading to the opposite chirality of the spin texture of the surface states [bottom panel of Fig. 4(b)]. For the superlattice with $P_b = -6.1\,\mu C/cm^2$ [Fig. 4(c)], the surface bands shift to lower energy than the case of $P_b = 0$, and the Dirac point of the Sn/Si-I termination is below the Fermi level. Like the case of $P_b = 6.1\,\mu C/cm^2$, for $P_b = -6.1\,\mu C/cm^2$, one Dirac point (from the Cs-I termination surface) is above the Fermi level, and the other Dirac point (from the Sn/Si-I termination surface) is below the Fermi level. While different from the case of $P_b = 6.1\,\mu C/cm^2$, for $P_b = -6.1\,\mu C/cm^2$, the surface bands from the Sn/Si-I termination (blue color) are much more flat, leading to them to be the outer branch bands, and the surface bands from the Cs-I termination become the inner branch bands at the Fermi level. Interestingly, in the superlattices with opposite directions of polarization, the chirality of the spin texture of surface states is the same, though the inner and outer branches of surface bands differ because of a difference in the surface termination [see the bottom panels of Figs. 4(a) and 4(c)]. Furthermore, the same chirality of the spin texture of surface states in the phases with opposite directions of polarization contrasts with the spin texture of states of Rashba effects, where the chirality is reversed when the polarization is switched [see Figs. 4(e) and 4(f)] [26,27,62–64].

Figure 4(d) further shows the energy of the Dirac point as a function of polarization. The energy of the Dirac point from the Cs-I termination surface is always above the Fermi level, while that from the Sn/Si-I termination is above the Fermi level for polarizations ranging between -4.7 to $4.7\,\mu C/cm^2$ and is below the Fermi level for polarizations larger in magnitude than $4.7\,\mu C/cm^2$. Therefore, the energy level of the Dirac point and the chirality of the spin texture are dependent on the

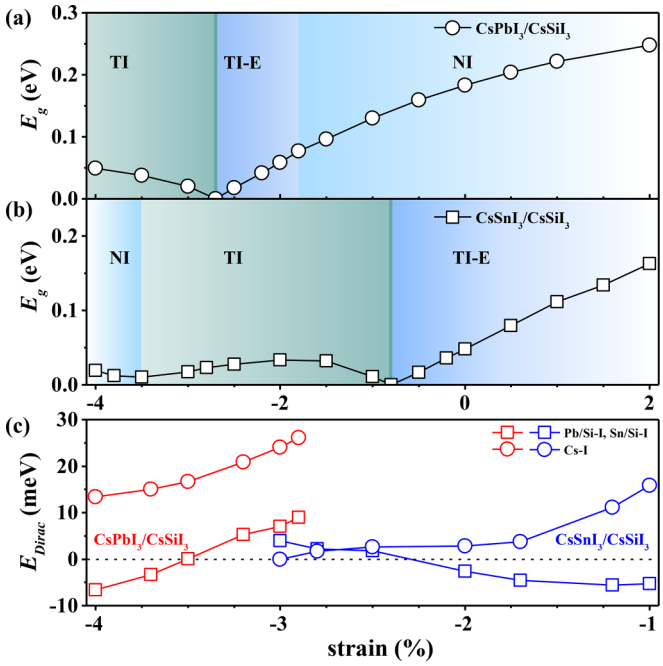

FIG. 5. Band gap and electronic phase of (a) $CsPbI_3/CsSiI_3$ and (b) $CsSnI_3/CsSiI_3$ superlattices as a function of epitaxial strain. $CsPbI_3/CsSiI_3$ can be normal insulator (NI), topological phase by decreasing the polarization (TI-E), and topological insulator (TI) phases depending on the strain. $CsSnI_3/CsSiI_3$ can be TI-E, TI, and NI for different strains. Light blue, blue, and green color represent NI, TI-E, and TI phases, respectively. (c) The energies of the Dirac point of surface states of $CsPbI_3/CsSiI_3$ and $CsSnI_3/CsSiI_3$ as a function of strain.

magnitude and direction of polarization. Note that one I ion in the Cs-I termination surface has one nearest neighboring Sn/Si ion, while one Sn/Si ion of the Sn/Si-I termination surface has five neighboring I ions. From the tight-binding model, the transfer integral of the states from the Cs-I termination surface is much smaller than that from the Sn/Si-I termination surface, leading to the surface states from the Sn/Si-I termination largely shifting their energy while those of the Cs-I termination slightly change their energy when changing the polarization. This electric field control of the Dirac point position in the band gap and altogether with the chirality of the spin texture of the surface state therefore provides a powerful and convenient toolkit to manipulate topological properties in ferroelectric perovskites.

Different from $CsSnI_3/CsSiI_3$ where a NI-TI phase transition occurs by reducing the polarization, $CsPbI_3/CsSiI_3$ is always NI in the whole range of polarization [see Fig. 3(a)] since it has a larger band gap (180 meV) than $CsSnI_3/CsSiI_3$ (48 meV). We now employ the epitaxial strain to engineer the band gap of the superlattices. Figure 5 displays the band gap of $CsPbI_3/CsSiI_3$ and $CsSnI_3/CsSiI_3$ as a function of such strain. The superlattices are NI (light blue color in Fig. 5) where the band gap decreases with the decrease of the strain from 2 to −2.7% for $CsPbI_3/CsSiI_3$ and from 2 to −0.8% for $CsSnI_3/CsSiI_3$. At the strain range from −1.8 and −2.7% for $CsPbI_3/CsSiI_3$ and from 2 and −0.8% for $CsSnI_3/CsSiI_3$, the band gap is small, and the phase NI can transform to phase TI by decreasing the polarization (phase TI-E, blue color in Fig. 5). At the critical strains where the band gaps for both superlattices are zero, the structures become Weyl semimetals. When the strain is smaller than the critical strain, the superlattices are TI phase (green color in Fig. 5). Additionally, $CsSnI_3/CsSiI_3$ becomes NI phase [light blue color in Fig. 5(b)] at the large compressive strain from −3.5 to −4% in Fig. 5(b).

Note that the energy of Dirac points of TI phases can be changed and even crosses the Fermi level when the strain changes. Figure 5(c) displays the energy of the Dirac point of the TI phase in $CsPbI_3/CsSiI_3$ and $CsSnI_3/CsSiI_3$ as a function of strain. For $CsPbI_3/CsSiI_3$, both Dirac points shift to lower energy when increasing the magnitude of compressive strain. Moreover, the energy of the Dirac point coming from the Pb/Si-I surface shifts from above to below the Fermi level and thus crosses the Fermi level. This shift of Dirac points is related to the change of Pb-I and Si-I bonds and the transfer integral between Pb/Si and I in the tight-binding model. For $CsSnI_3/CsSiI_3$, the Dirac point from the Cs-I termination decreases with the increase of magnitude of compressive strain and crosses the Fermi level at strain of −3%. Contrarily, the Dirac point from the Sn/Si-I termination increases with the increase of magnitude of compressive strain and crosses the Fermi level at strain of −2.3%. The shift of two Dirac energy levels of $CsSnI_3/CsSiI_3$ is not only dependent on the length of Sn-I/Si-I bonds but is also related to the polarization along the *b* and *c* directions. The polarization along the *b* direction decreases and the polarization along the *c* direction increases when increasing the magnitude of compressive strain (see Fig. S11 in the Supplemental Material [48]). At strain of about −2.5%, the polarizations along the *b* and *c* directions are equal, which may lead to similar energies of the Dirac points from Cs-I and Sn/Si-I terminations. Like the effect of polarization on the surface states in the TI-E phase [see Fig. 4(d)], the strain can shift the energy of the Dirac point and revert the chirality of the spin texture of surface states at the Fermi level. The topological phase and tunable surface states provide a convenient route to tune the topological order.

IV. CONCLUSION

In summary, we predicted a large Rashba effect and electric field induced topological order in halide perovskite superlattices of $CsPbI_3/CsSiI_3$ and $CsSnI_3/CsSiI_3$. Nonmonotonic behavior of the Rashba parameter as a function of polarization is found, and a large Rashba parameter can be achieved at a critical polarization where the NI-TI phase transition occurs. Moreover, in the TI phase, the spin texture of surface states and Dirac point energy are tunable by changing the polarization under electric field. The discovery of a class of ferroelectric materials with transition between NI and TI states and a tunable Rashba effect broadens the potential application of topological properties in electronics and spintronics.

ACKNOWLEDGMENTS

The authors thank the National Key R&D Program of China (Grants No. 2022YFB3807601 and No.

2020YFA0711504), the National Science Foundation of China (Grants No. 12274201, No. 12274174, No. 51725203, No. 51721001, No. 52003117, and No. 12104416), and the Natural Science Foundation of Jiangsu Province (Grant No. BK20200262). We are grateful to the HPCC resources of Nanjing University for the calculations. L.B. thanks the Vannevar Bush Faculty Fellowship Grant No. N00014-20-1-2834 from the Department of Defense and Award No. DMR-1906383 from the National Science Foundation AMASE-i Program (MonArk NSF Quantum Foundry).

[1] B. A. Bernevig, T. L. Hughes, and S.-C. Zhang, Science **314**, 1757 (2006).
[2] Y. Chen, J. G. Analytis, J.-H. Chu, Z. Liu, S.-K. Mo, X.-L. Qi, H. Zhang, D. Lu, X. Dai, Z. Fang *et al.*, Science **325**, 178 (2009).
[3] H. Zhang, C.-X. Liu, X.-L. Qi, X. Dai, Z. Fang, and S.-C. Zhang, Nat. Phys. **5**, 438 (2009).
[4] Z. Zhu, Y. Cheng, and U. Schwingenschlögl, Phys. Rev. Lett. **108**, 266805 (2012).
[5] A. Edström, D. Amoroso, S. Picozzi, P. Barone, and M. Stengel, Phys. Rev. Lett. **128**, 177202 (2022).
[6] N. S. Averkiev and L. E. Golub, Phys. Rev. B **60**, 15582 (1999).
[7] A. Manchon, H. C. Koo, J. Nitta, S. M. Frolov, and R. A. Duine, Nat. Mater. **14**, 871 (2015).
[8] H. Djani, A. C. Garcia-Castro, W. Y. Tong, P. Barone, E. Bousquet, S. Picozzi, and P. Ghosez, npj Quantum Mater. **4**, 51 (2019).
[9] K. Rubi, J. Gosteau, R. Serra, K. Han, S. W. Zeng, Z. Huang, B. Warot-Fonrose, R. Arras, E. Snoeck, A. M. Goiran *et al.*, npj Quantum Mater. **5**, 9 (2020).
[10] K. Yamauchi, P. Barone, and S. Picozzi, Phys. Rev. B **100**, 245115 (2019).
[11] X.-L. Qi, R. Li, J. Zang, and S.-C. Zhang, Science **323**, 1184 (2009).
[12] L. Fu and C. L. Kane, Phys. Rev. Lett. **100**, 096407 (2008).
[13] M. Konig, S. Wiedmann, C. Brune, A. Roth, H. Buhmann, L. W. Molenkamp, X.-L. Qi, and S.-C. Zhang, Science **318**, 766 (2007).
[14] I. Knez, R.-R. Du, and G. Sullivan, Phys. Rev. Lett. **107**, 136603 (2011).
[15] J. E. Hirsch, Phys. Rev. Lett. **83**, 1834 (1999).
[16] J. Sinova, S. O. Valenzuela, J. Wunderlich, C. H. Back, and T. Jungwirth, Rev. Mod. Phys. **87**, 1213 (2015).
[17] I. Sodemann, Z. Zhu, and L. Fu, Phys. Rev. X **7**, 041068 (2017).
[18] J. Nitta, F. E. Meijer, and H. Takayanagi, Appl. Phys. Lett. **75**, 695 (1999).
[19] D. Frustaglia and K. Richter, Phys. Rev. B **69**, 235310 (2004).
[20] K. Kondou, R. Yoshimi, A. Tsukazaki, Y. Fukuma, J. Matsuno, K. Takahashi, M. Kawasaki, Y. Tokura, and Y. Otani, Nat. Phys. **12**, 1027 (2016).
[21] S. Manipatruni, D. E. Nikonov, C.-C. Lin, T. A. Gosavi, H. Liu, B. Prasad, Y.-L. Huang, E. Bonturim, R. Ramesh, and I. A. Young, Nature (London) **565**, 35 (2019).
[22] D. Liu, Q. Li, H. Jing, and K. Wu, J. Phys. Chem. C **123**, 3795 (2019).
[23] P. Noël, F. Trier, L. M. Vicente Arche, J. Bréhin, D. C. Vaz, V. Garcia, S. Fusil, A. Barthélémy, L. Vila, M. Bibes *et al.*, Nature (London) **580**, 483 (2020).
[24] C. M. Acosta, A. Fazzio, G. M. Dalpian, and A. Zunger, Phys. Rev. B **102**, 144106 (2020).
[25] L. G. D. da Silveira, P. Barone, and S. Picozzi, Phys. Rev. B **93**, 245159 (2016).
[26] D. Di Sante, P. Barone, A. Stroppa, K. F. Garrity, D. Vanderbilt, and S. Picozzi, Phys. Rev. Lett. **117**, 076401 (2016).
[27] B. Monserrat, J. W. Bennett, K. M. Rabe, and D. Vanderbilt, Phys. Rev. Lett. **119**, 036802 (2017).
[28] Z. Zheng, Q. Ma, Z. Bi, S. de La Barrera, M.-H. Liu, N. Mao, Y. Zhang, N. Kiper, K. Watanabe, T. Taniguchi *et al.*, Nature (London) **588**, 71 (2020).
[29] S. Chen, S. Yuan, Z. Hou, Y. Tang, J. Zhang, T. Wang, K. Li, W. Zhao, X. Liu, L. Chen *et al.*, Adv. Mater. **33**, 2000857 (2021).
[30] D. Doennig, W. E. Pickett, and R. Pentcheva, Phys. Rev. B **89**, 121110(R) (2014).
[31] Y. Zhai, S. Baniya, C. Zhang, J. Li, P. Haney, C.-X. Sheng, E. Ehrenfreund, and Z. V. Vardeny, Sci. Adv. **3**, e1700704 (2017).
[32] E. Lafalce, E. Amerling, Z.-G. Yu, P. C. Sercel, L. Whittaker-Brooks, and Z. V. Vardeny, Nat. Commun. **13**, 483 (2022).
[33] J. Kaur and S. Chakraborty, ACS Appl. Energy Mater. **5**, 5579 (2022).
[34] X. Zhou, and Z. Zhang, AIP Adv. **10**, 085210 (2020).
[35] L. Leppert, S. E. Reyes-Lillo, and J. B. Neaton, J. Phys. Chem. Lett. **7**, 3683 (2016).
[36] H. Jin, J. Im, and A. J. Freeman, Phys. Rev. B **86**, 121102(R) (2012).
[37] R. Kashikar, B. Khamari, and B. R. K. Nanda, Phys. Rev. Mater. **2**, 124204 (2018).
[38] X. Y. Wang, X. Li, H. Tian, H. Sang, J.-M. Liu, and Y. Yang, J. Phys. Chem. C **126**, 20620 (2022).
[39] R. J. Sutton, M. R. Filip, A. A. Haghighirad, N. Sakai, B. Wenger, F. Giustino, and H. J. Snaith, ACS Energy Lett. **3**, 1787 (2018).
[40] T. Ye, X. Wang, K. Wang, S. Ma, D. Yang, Y. Hou, J. Yoon, K. Wang, and S. Priya, ACS Energy Lett. **6**, 1480 (2021).
[41] Z. Fang, M. Shang, X. Houa, Y. Zheng, Z. Du, Z. Yang, K.-C. Choua, W. Yang, Z. L. Wang, and Y. Yang, Nano Energy **61**, 389 (2019).
[42] S. K. Radha, C. Bhandari, and W. R. L. Lambrecht, Phys. Rev. Mater. **2**, 063605 (2018).
[43] L. Y. Huang and W. R. L. Lambrecht, Phys. Rev. B **93**, 195211 (2016).
[44] P. E. Blöchl, Phys. Rev. B **50**, 17953 (1994).
[45] G. Kresse and J. Furthmüller, Comput. Mater. Sci. **6**, 15 (1996).
[46] J. P. Perdew, A. Ruzsinszky, G. I. Csonka, O. A. Vydrov, G. E. Scuseria, L. A. Constantin, X. Zhou, and K. Burke, Phys. Rev. Lett. **100**, 136406 (2008).
[47] J. Heyd, G. E. Scuseria, and M. Ernzerhof, J. Chem. Phys. **118**, 8207 (2003).
[48] See Supplemental Material at http://link.aps.org/supplemental/10.1103/PhysRevB.108.045114 for details about the structure distortions, the ferroelectric and topological properties of superlattices, and the band structure from the HSE functional.
[49] I. Souza, N. Marzari, and D. Vanderbilt, Phys. Rev. B **65**, 035109 (2001).

[50] A. A. Mostofi, J. R. Yates, Y.-S. Lee, I. Souza, D. Vanderbilt, and N. Marzari, Comput. Phys. Commun. **178**, 685 (2008).
[51] Q. Wu, S. Zhang, H.-F. Song, M. Troyer, and A. A. Soluyanov, Comput. Phys. Commun. **224**, 405 (2018).
[52] A. M. Glazer, Acta Crystallogr. Sect. B **28**, 33894 (1972).
[53] L. Tao and E. Y. Tsymbal, Nat. Commun. **9**, 2763 (2018).
[54] F. Wang, I. Grinberg, and A. M. Rappe, Appl. Phys. Lett. **104**, 152903 (2014).
[55] R. F. Berger, C. J. Fennie, and J. B. Neaton, Phys. Rev. Lett. **107**, 146804 (2011).
[56] D. V. Cirlincione and R. F. Berger, Phys. Rev. B **103**, 045127 (2021).
[57] Y.-H. Meng, W. Bai, H. Gao, S.-J. Gong, J.-Q. Wang, C.-G. Duan, and J.-H. Chu, Nanoscale **9**, 17957 (2017).
[58] E. Plekhanov, P. Barone, D. Di Sante, and S. Picozzi, Phys. Rev. B **90**, 161108(R) (2014).
[59] M. S. Bahramy, B.-J. Yang, R. Arita, and N. Nagaosa, Nat. Commun. **3**, 679 (2012).
[60] M. S. Bahramy, R. Arita, and N. Nagaosa, Phys. Rev. B **84**, 041202(R) (2011).
[61] Y. Xia, D. Qian, D. Hsieh, A. Pal, L. Wray, H. Lin, A. Bansil, D. Grauer, Y. S. Hor, R. J. Cava *et al.*, Nat. Phys. **5**, 398 (2009).
[62] D. Di Sante, P. Barone, R. Bertacco, and S. Picozzi, Adv. Mater. **25**, 509 (2013).
[63] L. L. Tao, T. R. Paudel, A. A. Kovalev, and E. Y. Tsymbal, Phys. Rev. B **95**, 245141 (2017).
[64] M. Kim, J. Im, A. J. Freeman, J. Ihm, and H. Jin, Proc. Natl. Acad. Sci. USA **111**, 6900 (2014).